

# The Influence of Temperature on Ozone Production under varying $\text{NO}_x$ Conditions – a modelling study

J. Coates<sup>1</sup>, K. Mar<sup>1</sup> and T. Butler<sup>1</sup>

<sup>1</sup>Institute for Advanced Sustainability Studies, Potsdam, Germany

March 20, 2016

## Abstract

Surface ozone is a secondary air pollutant produced during the degradation of emitted volatile organic compounds (VOCs) in the presence of sunlight and nitrogen oxides ( $\text{NO}_x$ ). Temperature directly influences ozone production through speeding up the rates of the chemical reactions producing ozone and increasing the emissions of VOCs, such as isoprene, from vegetation. In this study, we used a box model to reproduce the non-linear relationship of ozone with  $\text{NO}_x$  and temperature from previous observational studies. An increase in ozone of up to 20 ppbv was due to faster reaction rates while increased isoprene emissions added a further 11 ppbv of ozone under high- $\text{NO}_x$  conditions. The increased rate of emitted VOC loss with temperature controlled the rate of  $\text{O}_x$  production with temperature increasing net  $\text{O}_x$  production by  $\sim 1$  molecule of  $\text{O}_x$  per loss of VOC. The rate of increase in ozone mixing ratios with temperature from our box model simulations was about half the rate of increase in ozone with temperature over central Europe compared to both observed values and WRF-Chem output. The missing sensitivity in our simulations compared to observations and 3D model output is related to not including stagnant atmospheric conditions in our experiment.

## 1 Introduction

Surface-level ozone ( $\text{O}_3$ ) is a secondary air pollutant formed during the photochemical degradation of volatile organic compounds (VOCs) in the presence of nitrogen oxides ( $\text{NO}_x \equiv \text{NO} + \text{NO}_2$ ). Due to the photochemical nature of ozone production it is strongly influenced by meteorological variables such as temperature (Jacob and Winner, 2009). Otero et al. (2016) showed that

temperature was a major meteorological driver for summertime ozone in many areas of central Europe.

Temperature primarily influences ozone production in two ways: speeding up the reaction rates of many chemical reactions leading to ozone production, and increasing emissions of VOCs from biogenic sources (BVOCs) (Sillman and Samson, 1995). While emissions of anthropogenic VOCs (AVOCs) are generally not dependent on temperature, evaporative emissions of AVOCs increase with temperature (Rubin et al., 2006). The review of Pusede et al. (2015) provides further details of the temperature-dependent processes impacting ozone production.

Regional modelling studies over the US (Sillman and Samson, 1995; Steiner et al., 2006; Dawson et al., 2007) examined the sensitivity of ozone production during a pollution episode to increased temperatures. These studies noted that increased temperatures (without changing VOC or  $\text{NO}_x$ -conditions) led to higher ozone levels, often exceeding local air quality guidelines. Sillman and Samson (1995) and Dawson et al. (2007) varied the temperature dependence of the PAN (peroxy acetyl nitrate) decomposition rate during simulations of the eastern US determining the sensitivity of ozone production with temperature to the PAN decomposition rate. In addition to noting the influence of PAN decomposition to ozone production, Steiner et al. (2006) correlated the increase in ozone mixing ratios with temperature over California to increased mixing ratios of formaldehyde, a secondary degradation product of many VOC and an important radical source. Steiner et al. (2006) also noted increased emissions of BVOCs at higher temperatures in urban areas with high  $\text{NO}_x$  emissions also increased ozone levels with temperature.

Pusede et al. (2014) used an analytical model constrained by observations over the San Joaquin Valley, California to infer a non-linear relationship of ozone production with temperature and  $\text{NO}_x$ , similar to the well-known non-linear relationship of ozone production on  $\text{NO}_x$  and VOC levels (Sillman, 1999). Moreover, Pusede et al. (2014) showed that temperature can be used as a surrogate for VOC levels when considering the relationship of ozone under different  $\text{NO}_x$  conditions.

Environmental chamber studies have also been used to analyse the relationship of ozone with temperature using a fixed mixture of VOCs. The chamber experiments of Carter et al. (1979) and Hatakeyama et al. (1991) showed increases in ozone from a VOC mix with temperature. Both studies compared the concentration time series of ozone and nitrogen-containing compounds ( $\text{NO}_x$ , PAN,  $\text{HNO}_3$ ) at various temperatures and linked the maximum in ozone concentration to the decrease in PAN concentrations at temperatures greater than 303 K.

Despite many studies considering the effects of temperature on ozone production from an observational and chamber study perspective, modelling studies focusing on the detailed chemical processes of the influence of temperature on ozone production under different  $\text{NO}_x$  conditions have not been performed (to our knowledge). The regional modelling studies described previously concentrated on reproducing ozone levels (using a single chemical mechanism) over regions with known meteorology and  $\text{NO}_x$  conditions then varying the temperature. These modelling studies did not consider the relationship of ozone with  $\text{NO}_x$  and temperature. The review of Pusede et al. (2015) also highlights a lack of modelling studies looking at the non-linear relationship of ozone on temperature under different  $\text{NO}_x$  conditions.

Comparisons of different chemical mechanisms, such as Emmerson and Evans (2009) and Coates and Butler (2015), showed that different representations of tropospheric chemistry influenced ozone production. Neither of these studies examined the ozone-temperature relationship differences between chemical mechanisms. Furthermore, Rasmussen et al. (2013) acknowledged that the modelled ozone-temperature relationship may be sensitive to the choice of chemical mechanism and recommended investigating this sensitivity. Comparing the ozone-temperature relationship predicted by different chemical mechanisms is potentially important for modelling of future air quality due to the expected increase in heatwaves (Karl and Trenberth, 2003).

In this study, we use an idealised box model to determine how ozone levels vary with temperature under different  $\text{NO}_x$  conditions. We determine whether faster chemical reaction rates or increased BVOC emissions have a greater influence on instantaneous ozone production with higher temperature under different  $\text{NO}_x$  conditions. Furthermore, we compare the ozone-temperature relationship produced by different chemical mechanisms.

## 2 Methodology

### 2.1 Model Setup

We used the MECCA box model (Sander et al., 2005) to determine the important gas-phase chemical processes for ozone production under different temperatures and  $\text{NO}_x$  conditions. The MECCA box model was set up as described in Coates and Butler (2015) and updated to include vertical mixing with the free troposphere using a diurnal cycle for the PBL height. The supplementary material includes further details of these updates.

Simulations broadly representative of urban conditions in central Europe with equinoctical

conditions were performed. The simulations started at 06:00 with a total run time of two days. Methane was fixed at 1.7 ppmv throughout the model run, carbon monoxide (CO) and ozone were initialised at 200 ppbv and 40 ppbv and then allowed to evolve freely throughout the simulation. All VOC emissions were held constant until noon of first day simulating a plume of freshly-emitted VOC.

Separate box model simulations were performed by systematically varying the temperature between 288 and 313 K (15 – 40 °C) in steps of 0.5 K. NO emissions were systematically varied between  $5.0 \times 10^9$  and  $1.5 \times 10^{12}$  molecules (NO)  $\text{cm}^{-2} \text{s}^{-1}$  at each temperature used in this study. At 20 °C, these NO emissions corresponded to peak  $\text{NO}_x$  mixing ratios of 0.02 ppbv and 10 ppbv respectively, this range of  $\text{NO}_x$  mixing ratios covers the  $\text{NO}_x$  conditions found in pristine and urban conditions (von Schneidemesser et al., 2015).

All simulations were repeated using different chemical mechanisms to investigate whether the relationship between ozone, temperature and  $\text{NO}_x$  changes using different representations of ozone production chemistry. The reference chemical mechanism was the near-explicit Master Chemical Mechanism, MCMv3.2, (Jenkin et al., 1997, 2003; Saunders et al., 2003; Rickard et al., 2015). The reduced chemical mechanisms in our study were Common Representative Intermediates, CRIV2 (Jenkin et al., 2008), Model for ozone and related chemical tracers, MOZART-4 (Emmons et al., 2010), Regional Acid Deposition Model, RADM2 (Stockwell et al., 1990) and the Carbon Bond Mechanism, CB05 (Yarwood et al., 2005). Coates and Butler (2015) described the implementation of these chemical mechanisms in MECCA. These reduced chemical mechanisms were chosen as they are commonly used by modelling groups in 3D regional and global models (Baklanov et al., 2014).

Model runs were repeated using a temperature-dependent and temperature-independent source of BVOC emissions to determine the relative importance of increased emissions of BVOC and faster reaction rates of chemical processes for the increase of ozone with temperature. MEGAN2.1 (Guenther et al., 2012) specified the temperature-dependent BVOC emissions of isoprene, Sect. 2.3 provides further details. As isoprene emissions are the most important on the global scale, we considered only isoprene emissions from vegetation (Guenther et al., 2006). Only isoprene emissions were dependent on temperature, all other emissions were constant in all simulations. In reality, many other BVOC are emitted from varying vegetation types (Guenther et al., 2006) and increased temperature can also increase BVOC emissions through increased evaporation (Rubin et al., 2006).

Table 1: Total AVOC emissions in 2011 in tonnes from each anthropogenic source category assigned from TNO-MACC\_III emission inventory and temperature-independent BVOC emissions in tonnes from Benelux region assigned from EMEP. The allocation of these emissions to MCMv3.2, CRIV2, CB05, MOZART-4 and RADM2 species are found in the supplementary material.

Source Category	Total Emissions	Source Category	Total Emissions
Public Power	13755	Road Transport: Diesel	6727
Residential Combustion	21251	Road Transport: Others	1433
Industry	62648	Road Transport: Evaporation	2327
Fossil Fuel	15542	Non-road Transport	17158
Solvent Use	100826	Waste	1342
Road Transport: Gasoline	24921	BVOC	10702

## 2.2 VOC Emissions

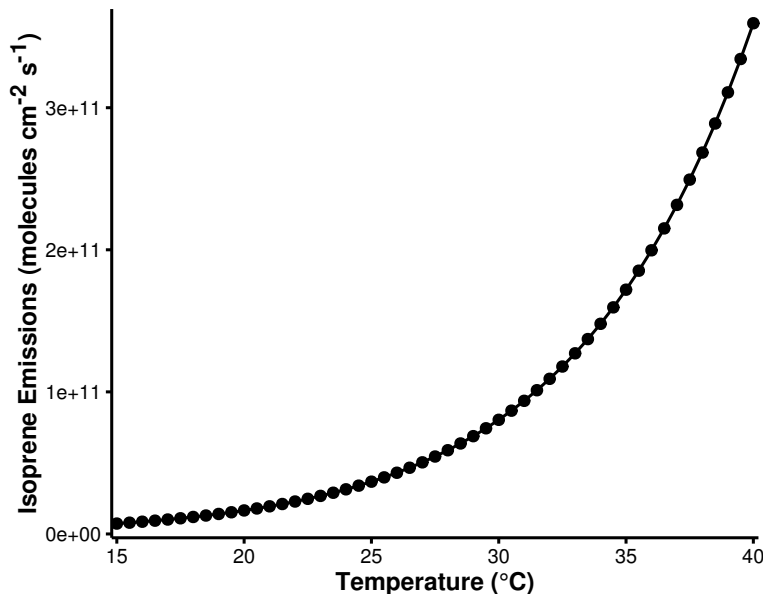
Emissions of urban AVOC over central Europe were taken from TNO-MACC\_III emission inventory for the Benelux (Belgium, Netherlands and Luxembourg) region for the year 2011. TNO-MACC\_III is the updated TNO-MACC\_II emission inventory created using the same methodology as Kuenen et al. (2014) and based upon improvements to the existing emission inventory during AQMEII-2 (Pouliot et al., 2015).

Temperature-independent emissions of isoprene and monoterpenes from biogenic sources were calculated as a fraction of the total AVOC emissions from each country in the Benelux region. This data was obtained from the supplementary data available from the EMEP (European Monitoring and Evaluation Programme) model (Simpson et al., 2012). Temperature-dependent emissions of isoprene are detailed in Sect. 2.3.

Table 1 shows the quantity of VOC emissions from each source category and the temperature-independent BVOC emissions. These AVOC emissions were assigned to chemical species and groups based on the profiles provided by TNO. Most individual chemical species are represented by the MCMv3.2, otherwise the individual contributions of a group of VOC were further split into individual components using the detailed speciation of Passant (2002). For example, ‘xylenes’ are one of the component chemical groups in many source categories but the MCMv3.2 treats xylenes as the individual isomers (m-, o-, p-xylene) and the contributions of the individual isomers to a source category was provided by Passant (2002). This approach was also used in von Schneidmesser et al. (2016) to allocate AVOC emissions from different solvent sector speciations to MCMv3.2 species.

For simulations done with other chemical mechanisms, the VOC emissions represented by the MCMv3.2 were mapped to the mechanism species representing VOC emissions in each reduced

Figure 1: The estimated isoprene emissions (molecules isoprene  $\text{cm}^{-2} \text{s}^{-1}$ ) using MEGAN2.1 at each temperature used in the study.



chemical mechanism based on the recommendations of the source literature and Carter (2015). The VOC emissions in the reduced chemical mechanisms were weighted by the carbon numbers of the MCMv3.2 species and the emitted mechanism species, thus keeping the amount of emitted reactive carbon constant between simulations. The supplementary data outlines the primary VOC and calculated emissions with each chemical mechanism.

### 2.3 Temperature Dependent Isoprene Emissions

Temperature-dependent emissions of isoprene were estimated using the MEGAN2.1 algorithm for calculating the emissions of VOC from vegetation (Guenther et al., 2012). Emissions from nature are dependent on many variables including temperature, radiation and age but for the purpose of our study all variables except temperature were held constant.

The MEGAN2.1 parameters were chosen to give similar isoprene mixing ratios at 20 °C to the temperature-independent emissions of isoprene in order to compare the effects of increased isoprene emissions with temperature. The estimated emissions of isoprene with MEGAN2.1 using these assumptions are illustrated in Fig. 1 and show the expected exponential increase in isoprene emissions with temperature (Guenther et al., 2006).

The estimated emissions of isoprene at 20 °C lead to 0.07 ppbv of isoprene in our simulations while at 30 °C, the increased emissions of isoprene using MEGAN2.1 estimations lead to 0.35 ppbv of isoprene in the model. A measurement campaign over Essen, Germany (Wagner and Kuttler,

Table 2: Increase in mean ozone mixing ratio (ppbv) due to chemistry and temperature-dependent isoprene emissions from the reference temperature (20 °C) at 40 °C in the NO<sub>x</sub>-regimes of Fig. 3.

Chemical Mechanism	Source of Difference	Increase in Ozone from 20 °C at 40 °C (ppbv)		
		Low-NO <sub>x</sub>	Maximal-O <sub>3</sub>	High-NO <sub>x</sub>
MCMv3.2	Isoprene Emissions Chemistry	4.6	7.7	10.6
		6.8	12.5	15.2
CRIV2	Isoprene Emissions Chemistry	4.8	7.9	10.8
		6.0	11.1	13.7
MOZART-4	Isoprene Emissions Chemistry	4.1	6.7	10.0
		6.0	10.2	12.3
CB05	Isoprene Emissions Chemistry	4.6	7.4	9.8
		9.3	16.0	19.9
RADM2	Isoprene Emissions Chemistry	3.8	5.7	7.8
		8.6	14.1	17.3

2014) measured 0.1 ppbv of isoprene at temperature 20 °C and 0.3 ppbv of isoprene were measured at 30 °C. The similarity of the simulated and observed isoprene mixing ratios indicates that the MEGAN2.1 variables chosen for calculating the temperature-dependent emissions of isoprene were suitable for simulating urban conditions over central Europe.

### 3 Results and Discussion

#### 3.1 Ozone as a Function of NO<sub>x</sub> and Temperature

Figure 2 depicts the peak mixing ratio of ozone of each simulation as a function of the total NO<sub>x</sub> emissions and temperature on the first day of simulations when using a temperature-independent and temperature-dependent source of isoprene emissions for each chemical mechanism. A non-linear relationship of ozone mixing ratios with NO<sub>x</sub> and temperature is reproduced by each chemical mechanism. This non-linear relationship is similar to that determined by Pusede et al. (2014) using an analytical model constrained to observational measurements over the San Joaquin Valley, California.

Higher ozone mixing ratios are produced when using a temperature-dependent source of isoprene emissions (Fig. 2). The highest mixing ratios of ozone are produced at high temperatures and moderate emissions of NO<sub>x</sub> regardless of the temperature dependence of isoprene emissions. Conversely, the least amount of ozone is produced with low emissions of NO<sub>x</sub> over the whole temperature range (15 – 40 °C) when using both a temperature-independent and temperature-dependent source of isoprene emissions.

The contours of ozone mixing ratios as a function of NO<sub>x</sub> and temperature can be split into three NO<sub>x</sub> regimes (Low-NO<sub>x</sub>, Maximal-O<sub>3</sub> and High-NO<sub>x</sub>), similar to the NO<sub>x</sub> regimes defined

Figure 2: Contours of peak ozone mixing ratios (ppbv) as a function of the total  $\text{NO}_x$  emissions on the first day and temperature for each chemical mechanism using a temperature-dependent and temperature-independent source of isoprene emissions. The contours can be split into three separate regimes: High- $\text{NO}_x$ , Maximal- $\text{O}_3$  and Low- $\text{NO}_x$  indicated in the figure.

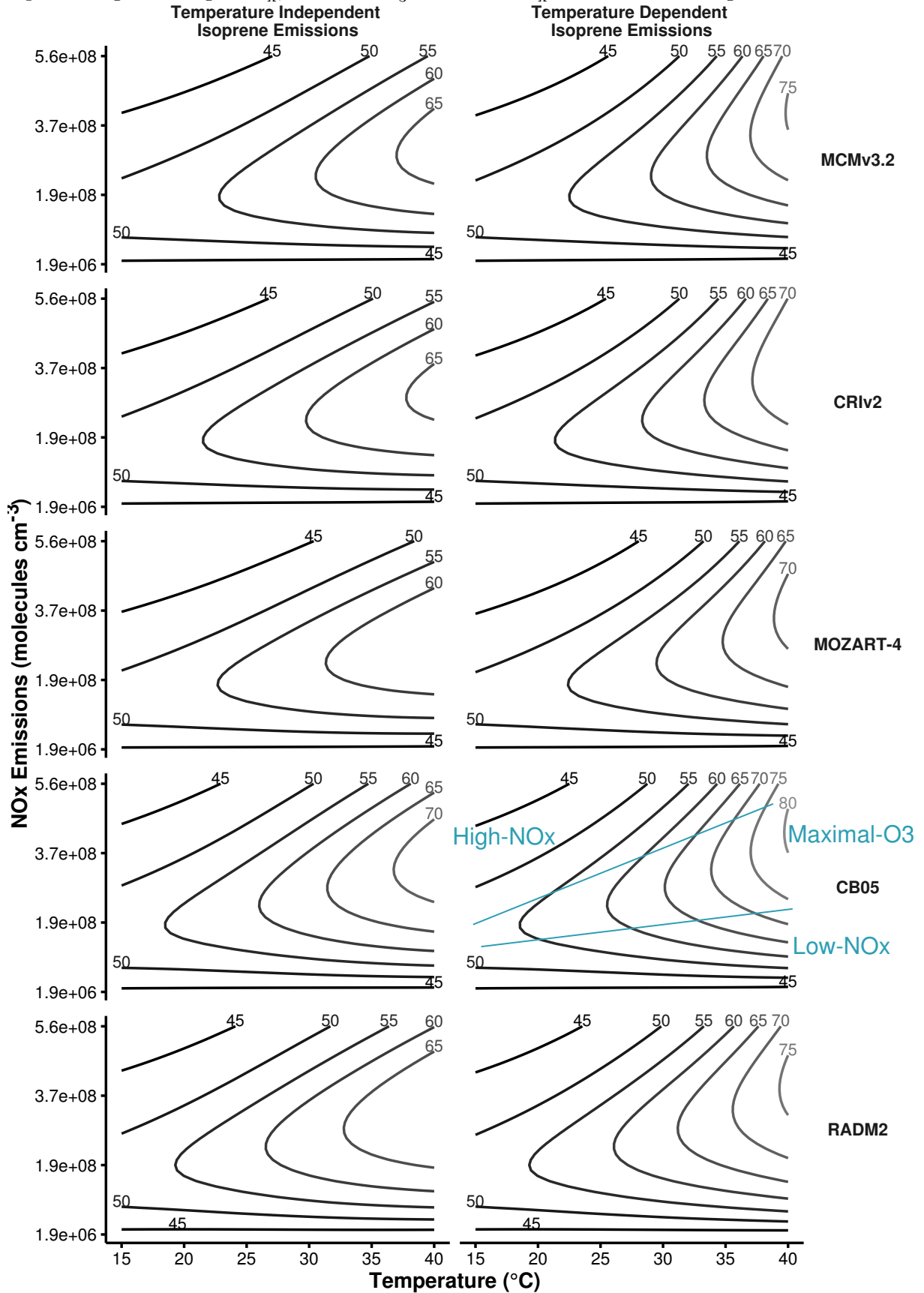
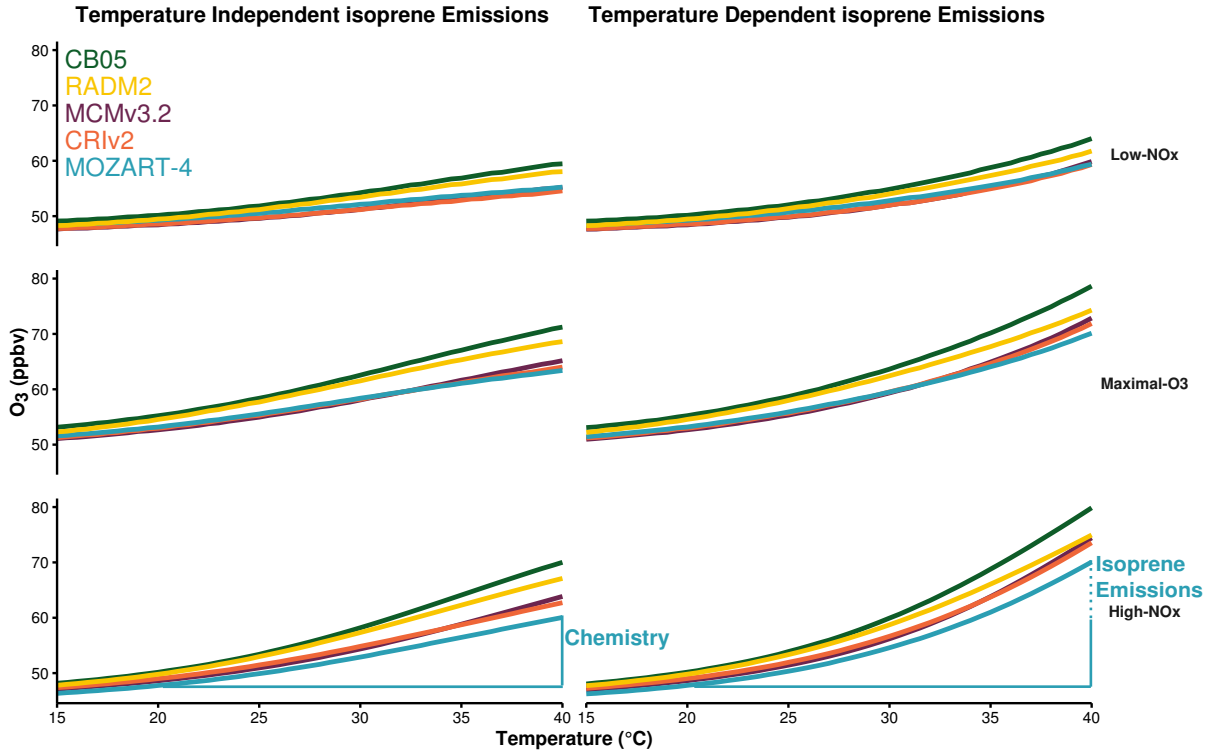




Figure 3: Mean ozone mixing ratios (ppbv) at each temperature are allocated to the different  $\text{NO}_x$ -regimes of Fig. 2. The differences in ozone mixing ratios due to chemistry (solid line) and isoprene emissions (dotted line) are represented graphically for MOZART-4 with High- $\text{NO}_x$  conditions. Table 2 details the differences for all chemical mechanisms and  $\text{NO}_x$ -conditions.



for the non-linear relationship of ozone with VOC and  $\text{NO}_x$ . The Low- $\text{NO}_x$  regime corresponds with regions with little increase in ozone with temperature, also called the  $\text{NO}_x$ -sensitive regime. The High- $\text{NO}_x$  (or  $\text{NO}_x$ -saturated) regime is when ozone levels increase rapidly with temperature. The contour ridges correspond to regions of maximal ozone production; this is the Maximal- $\text{O}_3$  regime. Pusede et al. (2014) showed that temperature can be used as a proxy for VOC, thus we assigned the ozone mixing ratios from each box model simulation to a  $\text{NO}_x$  regime based on the ratio of  $\text{HNO}_3$  to  $\text{H}_2\text{O}_2$ . This ratio was used by Sillman (1995) to designate ozone to  $\text{NO}_x$  regimes based on  $\text{NO}_x$  and VOC levels. The Low- $\text{NO}_x$  regime corresponds to  $\text{H}_2\text{O}_2:\text{HNO}_3$  ratios less than 0.5, the High- $\text{NO}_x$  regime corresponds to ratios larger than 0.3 and ratios between 0.3 and 0.5 correspond to the Maximal- $\text{O}_3$  regime.

The peak ozone mixing ratio from each simulation was assigned to a  $\text{NO}_x$  regime based on the  $\text{H}_2\text{O}_2:\text{HNO}_3$  ratio of that simulation. The ozone mixing ratios assigned to each  $\text{NO}_x$  regime at each temperature were averaged, this is illustrated in Figure 3 for each chemical mechanism and each type of isoprene emissions (temperature independent and temperature dependent). We define the absolute increase in ozone from 20 °C to 40 °C due to faster reaction rates as the difference

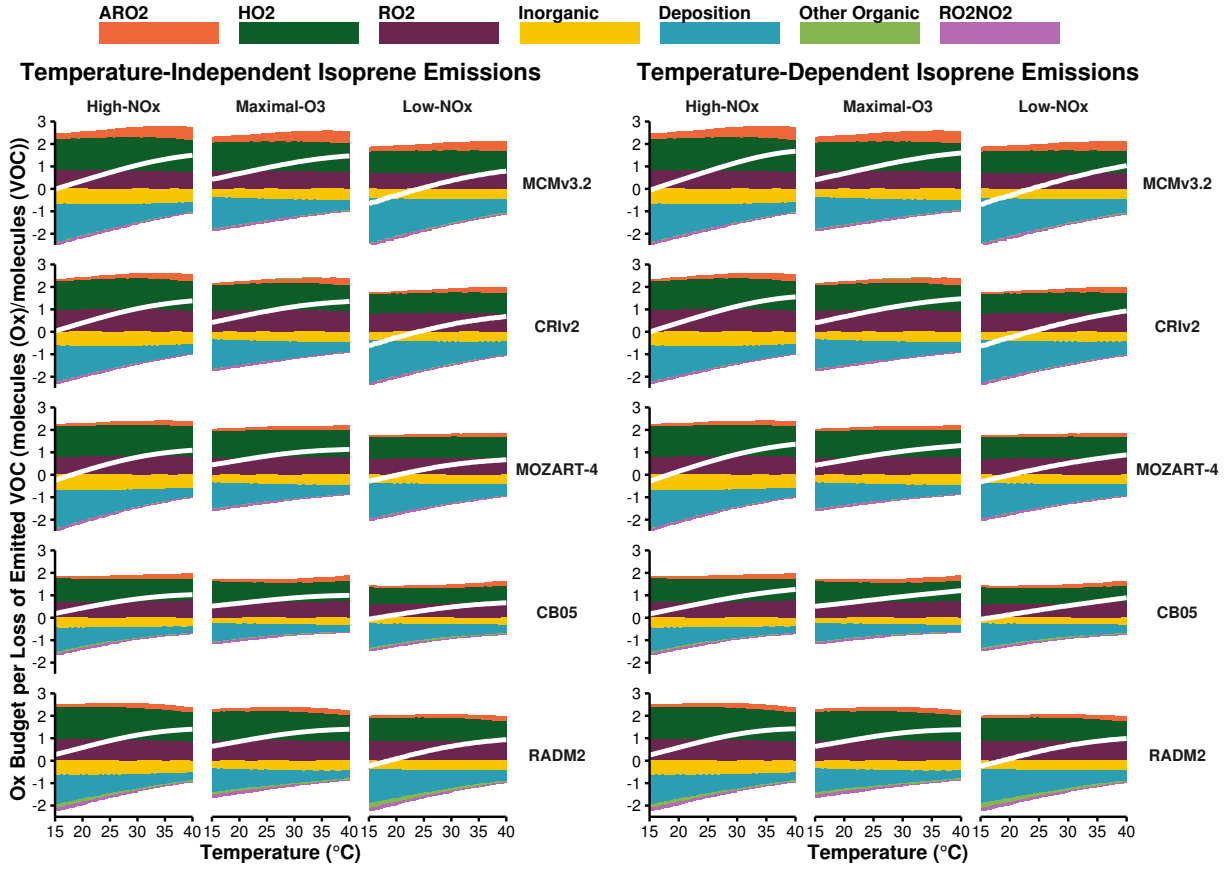
between ozone mixing ratios from 20 °C to 40 °C when using a temperature-independent source of isoprene emissions. When using a temperature-dependent source of isoprene emissions, the difference in ozone mixing ratios from 20 °C to 40 °C minus the increase due to faster chemistry, gives the absolute increase in ozone mixing ratios from increased isoprene emissions. These differences are represented graphically in Fig. 3 and summarised in Table 2.

Table 2 shows that the absolute increase in ozone with temperature due to chemistry (i.e. faster reaction rates) is larger than the absolute increase in ozone due to increased isoprene emissions for each chemical mechanism and each NO<sub>x</sub> regime. In all cases the absolute increase in ozone is largest under High-NO<sub>x</sub> conditions and lowest with Low-NO<sub>x</sub> conditions (Fig. 3 and Table 2). The increase in ozone mixing ratio from 20 °C to 40 °C due to faster reaction rates with High-NO<sub>x</sub> conditions is almost double that with Low-NO<sub>x</sub> conditions. In the Low-NO<sub>x</sub> regime, the increase of ozone with temperature using the reduced chemical mechanisms (CRIV2, MOZART-4, CB05 and RADM2) is similar to that from the MCMv3.2. Larger differences occur in the Maximal-O<sub>3</sub> and High-NO<sub>x</sub> regimes.

All reduced chemical mechanisms except RADM2 have similar increases in ozone due to increased isoprene emissions as the MCMv3.2 (Table 2). RADM2 produces 3 ppbv less ozone than the MCMv3.2 due to increased isoprene emissions in each NO<sub>x</sub> regime, indicating that this difference is due the representation of isoprene degradation chemistry in RADM2.

The Tagged Ozone Production Potential (TOPP) defined in Butler et al. (2011) is a measure of the number of molecules of ozone produced per molecule of VOC emitted. Coates and Butler (2015) compared ozone production in different chemical mechanisms to the MCMv3.2 using TOPPs and showed that less ozone is produced per molecule of isoprene emitted using RADM2 than with MCMv3.2. The degradation of isoprene has been extensively studied and it is well-known that methyl vinyl ketone (MVK) and methacrolein are signatures of isoprene degradation (Atkinson, 2000). All chemical mechanisms in our study except RADM2 explicitly represent MVK and methacrolein (or in the case of CB05, a lumped species representing both these secondary degradation products). RADM2 does not represent methacrolein and the mechanism species representing ketones (KET) is a mixture of acetone and methyl ethyl ketone (MEK) (Stockwell et al., 1990). Thus the secondary degradation of isoprene in RADM2 is unable to represent the ozone production from the further degradation of the signature secondary degradation products of isoprene, MVK and methacrolein. Updated versions of RADM2, RACM (Stockwell et al., 1997) and RACM2 (Goliff et al., 2013), sequentially included methacrolein and

Figure 4: Day-time budgets of  $O_x$  normalised by the total oxidation rate of emitted VOC in the  $NO_x$ -regimes of Fig. 3. The white line indicates net production or consumption of  $O_x$ . The net contribution of reactions to  $O_x$  budgets are allocated to categories of deposition, inorganic reactions, peroxy nitrates ( $RO_2NO_2$ ), reactions of NO with  $HO_2$ , alkyl peroxy radicals ( $RO_2$ ) and acyl peroxy radicals ( $ARO_2$ ). All other reactions are allocated to the ‘Other Organic’ category.



MVK and with these updates the TOPP value of isoprene approached that of the MCMv3.2 (Coates and Butler, 2015).

### 3.2 Ozone Production Budgets

In order to understand the temperature dependence of the ozone production directly, we examine the day-time production and consumption budgets of  $O_x$  ( $\equiv O_3 + NO_2 + O + O(^1D)$ ) normalised by the total rate of oxidation of the emitted VOC (Fig. 4). The  $O_x$  budgets are assigned to each  $NO_x$  regime for each chemical mechanism and type of isoprene emissions. The budgets are allocated to the net contribution of major categories, where ‘ $HO_2$ ’, ‘ $RO_2$ ’, ‘ $ARO_2$ ’ represent the reactions of NO with  $HO_2$ , alkyl peroxy radicals and acyl peroxy radicals respectively. ‘ $RO_2NO_2$ ’ represents the net effects of peroxy nitrates, ‘Deposition’ represents ozone deposition, ‘Inorganic’ is all other inorganic contributions to  $O_x$  production. Any other remaining organic reactions are included in the ‘Other Organic’ category. Figure 4 also illustrates the net production or consumption of  $O_x$  in each case.

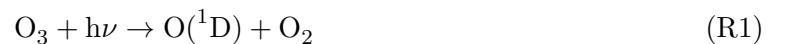
With each chemical mechanism, NO<sub>x</sub>-condition and type of isoprene emissions (temperature dependent and temperature independent), the net O<sub>x</sub> production efficiency increases from 20 °C to 40 °C by  $\sim 1$  molecule of O<sub>x</sub> per molecule of VOC oxidised (Fig. 4). The net O<sub>x</sub> production per oxidation of emitted VOC increases with temperature due to a decrease in ozone deposition per molecule of VOC oxidation with temperature. Ozone deposition is treated as a temperature-independent process in the boxmodel with a deposition velocity of 0.5 cm s<sup>-1</sup>. The deposition velocity ( $v_d$ ) is typically modelled using a resistance model with

$$v_d = (R_a + R_b + R_c)^{-1}$$

where  $R_a$ ,  $R_b$  and  $R_c$  are the aerodynamic, quasi-laminar boundary layer and canopy resistances, and the canopy resistance is influenced by meteorological variables such as temperature (Mészáros et al., 2009). Thus in reality, the temperature dependence of ozone deposition over vegetation all may also influence ozone production.

As the production efficiency of O<sub>x</sub> remains constant with temperature ( $\sim 2$  molecules of O<sub>x</sub> per molecule of VOC oxidised, Fig. 4), the rate of O<sub>x</sub> production is controlled by the oxidation of VOCs. Faster oxidation of VOCs with temperature speeds up the production of peroxy radicals increasing ozone production when peroxy radicals react with NO to produce NO<sub>2</sub>. The review of Pusede et al. (2015) acknowledged the importance of organic reactivity and radical production to the ozone-temperature relationship. Also, the modelling study of Steiner et al. (2006) noted that the increase in initial oxidation rates of VOCs with temperature leads to increased formaldehyde concentrations and in turn an increase of ozone as formaldehyde is an important source of HO<sub>2</sub> radicals.

Increased VOC oxidation with temperature is tied to faster reaction rates and increased levels of OH with temperature. An increase of ozone with temperature goes hand in hand with an increase of OH with temperature since ozone photolysis is the dominant source of OH radicals in the atmosphere.



Furthermore, enhanced formaldehyde production from the faster degradation of VOCs increases HO<sub>2</sub> formation speeding up the reaction rate of the reaction of HO<sub>2</sub> and NO. (R3) is responsible for both ozone production (through NO<sub>2</sub> production) and OH recycling further

Table 3: Slopes ( $m_{O_3-T}$ , ppbv per  $^{\circ}C$ ) of the linear fit to MDA8 values of ozone and temperature correlations in Fig. 5, indicating the increase of MDA8 in ppbv of ozone per  $^{\circ}C$ . The slope of the observational data is 2.15 ppbv/ $^{\circ}C$  and the slope of the WRF-Chem output is 2.05 ppbv/ $^{\circ}C$ .

Mechanism	Isoprene Emissions	Low- $NO_x$		Maximal- $O_3$		High- $NO_x$	
		Mixing	Stagnation	Mixing	Stagnation	Mixing	Stagnation
MCMv3.2	Temperature Independent	0.28	1.01	0.51	1.36	0.59	0.96
	Temperature Dependent	0.42	1.48	0.74	2.16	0.93	2.63
CRIV2	Temperature Independent	0.25	0.93	0.47	1.27	0.55	0.88
	Temperature Dependent	0.40	1.44	0.71	2.09	0.90	2.52
MOZART-4	Temperature Independent	0.25	0.97	0.44	1.21	0.49	0.59
	Temperature Dependent	0.38	1.43	0.65	1.98	0.81	2.05
CB05	Temperature Independent	0.39	1.30	0.67	1.72	0.79	1.45
	Temperature Dependent	0.52	1.72	0.89	2.44	1.12	2.94
RADM2	Temperature Independent	0.37	1.31	0.61	1.64	0.70	1.28
	Temperature Dependent	0.48	1.68	0.79	2.22	0.97	2.49

illustrating the strong coupling of ozone and OH production.

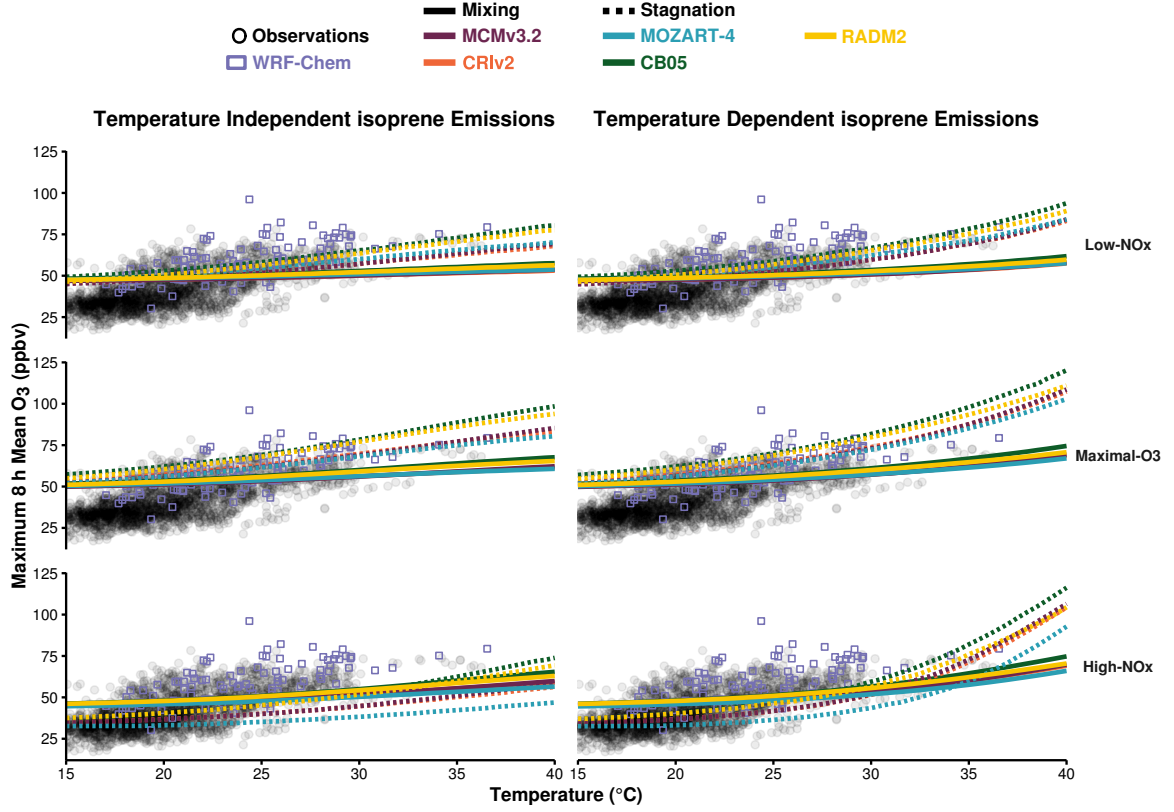


The net effect of peroxy nitrates on  $O_x$  budgets in our study is negligible, contributing to a loss of  $\sim 0.1$  molecules of  $O_x$  per VOC oxidised from 20  $^{\circ}C$  to 40  $^{\circ}C$  (Fig. 4). Peroxy nitrates are produced from the reactions of acyl peroxy radicals with  $NO_2$  and are an important reservoir of peroxy radicals and  $NO_x$ . The decomposition rate of peroxy nitrates is strongly temperature dependent and at higher temperatures the faster decomposition rate of  $RO_2NO_2$  leads to faster release of peroxy radicals and  $NO_2$ . Dawson et al. (2007) attributed the increase in maximum 8 h ozone mixing ratios with temperature during a modelling study over the eastern US to the decrease in PAN lifetime with temperature. Steiner et al. (2006) also recognised that the decrease in PAN lifetime with temperature contributed to the increase of ozone with temperature concluding that the combined effects of increased oxidation rates of VOC and faster PAN decomposition increased the production of ozone with temperature. In our results (Fig. 4), the net effect of  $RO_2NO_2$  is small since the decomposition rate is almost exactly balanced by the production from  $RO_2 + NO_2$ .

### 3.3 Comparison to Observations and 3D Model Simulations

This section compares the results from our idealised box model simulations to real-world observations and model output from a 3D model. Otero et al. (2016) showed that over the summer (JJA) months, temperature is the main meteorological driver of ozone production over many regions of central Europe using the interpolated observations of the maximum daily 8 h mean (MDA8) of ozone from Schnell et al. (2015) and the meteorological observational data set

Figure 5: MDA8 values of ozone from the box model simulations allocated to the different  $\text{NO}_x$  regimes for each chemical mechanism with mixing (solid lines) and stagnant conditions (dashed lines). The box model ozone-temperature correlation is compared to the summer 2007 observational data (black circles) and WRF-Chem output (purple boxes).



of the ERA-Interim re-analysis. Model output from the 3D WRF-Chem regional model using MOZART-4 chemistry set-up over the European domain for simulations of the year 2007 from Mar et al. (2016) was used to further compare the box model simulations to a model including more meteorological processes than our box model.

Figure 5 compares the observational and WRF-Chem data from summer 2007 over central and eastern Germany, where summertime ozone values are driven by temperature (Otero et al., 2016), to the maximum 8 h mean ozone from the box model simulations for each chemical mechanism. Table 3 summarises the slopes ( $m_{\text{O}_3\text{-T}}$ ) of the linear fits of each ozone-temperature correlation displayed in Fig. 5 in ppbv of ozone per °C determining the rate of change of ozone with temperature.

Despite, a high bias in simulated ozone in WRF-Chem, the rate of change of ozone with temperature from the WRF-Chem simulations (2.05 ppbv/°C) is similar to the rate of change of ozone with temperature from the observed data (2.15 ppbv/°C). The differences in ozone production between the different chemical mechanisms with the box model are small compared to the spread of the observational and WRF-Chem data. A temperature-dependent source of

isoprene with high-NO<sub>x</sub> conditions produces the most similar ozone-temperature slope to the observational data but this is still lower than the observed ozone-temperature slope by a factor of two. In particular, the box model simulations over-predict the ozone values at lower temperatures and under-predict the ozone values at higher temperatures compared to the observed data.

The main reason for the box model simulations being less sensitive to temperature than the observations and WRF-Chem is related to the set-up of the box model. In our simulations, we focused on instantaneous production of ozone from a freshly-emitted source of VOC and do not consider stagnant atmospheric conditions characterised by high temperatures and low wind speeds slowing the transport of ozone and its precursors away from sources. Otero et al. (2016) showed that the previous day’s ozone was also an important driver for observed ozone production over Europe and Jacob et al. (1993) correlated high-ozone episodes in the summer over eastern US to regional stagnation.

Stagnation is an example of how the coupling of meteorological variables to each other (in this case temperature and wind speed) impact ozone production. In observational studies, which consider the total derivative of ozone with temperature, the direct effects of temperature (e.g. increasing reaction rates, emissions from vegetation) and indirect (e.g. heatwaves characterised by low wind speeds) effects of temperature on ozone are not easily separated. In other words, observational studies represent the total derivative of ozone with temperature while models consider the partial derivatives of the temperature-dependent processes influencing ozone (Rasmussen et al., 2013).

$$\frac{d[\text{O}_3]}{dT} = \frac{\partial[\text{O}_3]}{\partial[\text{BVOC}]}\frac{\partial[\text{BVOC}]}{\partial T} + \frac{\partial[\text{O}_3]}{\partial\text{Chemistry}}\frac{\partial\text{Chemistry}}{\partial T} + \frac{\partial[\text{O}_3]}{\partial\text{Stagnation}}\frac{\partial\text{Stagnation}}{\partial T} + \dots$$

3D models such as WRF-Chem that can simulate more realistic atmospheric conditions would play a valuable role for future work evaluating the ozone-temperature relationship at different NO<sub>x</sub> conditions at a regional scale.

## 4 Conclusions

In this study, we determined the effects of temperature on ozone production using a box model over a range of temperatures and NO<sub>x</sub> conditions with a temperature-independent and temperature-dependent source of isoprene emissions. These simulations were repeated using reduced chemical mechanism schemes (CRIV2, MOZART-4, CB05 and RADM2) typically used in 3D models and compared to the near-explicit MCMv3.2 chemical mechanism.

Each chemical mechanism produced a non-linear relationship of ozone with temperature and  $\text{NO}_x$  with the most ozone produced at high temperatures and moderate emissions of  $\text{NO}_x$ . Conversely, lower  $\text{NO}_x$  levels led to a minimal increase of ozone with temperature. Thus air quality in a future with higher temperatures would benefit from dramatical reductions in  $\text{NO}_x$  emissions.

Faster reaction rates at higher temperatures were responsible for a greater absolute increase in ozone than increased isoprene emissions. The increase in VOC loss with temperature was the dominant process increasing ozone production with temperature. The increase of ozone with temperature is coupled with increasing OH with temperature increasing VOC loss at higher temperatures. Enhanced VOC loss at higher temperatures increased the production of peroxy radicals, leading to ozone production.

The rate of change of ozone with temperature using observational data (ERA-Interim) over Europe was twice as high as when using the box model. This was consistent with our box model setup not representing stagnant atmospheric conditions that are inherently included in observational data and models including meteorology, such as WRF-Chem. Future work looking at the influence of temperature on ozone should include stagnant conditions to represent more realistic atmospheric conditions. Any modelling work addressing this should also consider a range of  $\text{NO}_x$  conditions as this strongly influenced the amount of ozone produced in our study.

## Acknowledgements

The authors would like to thank Noelia Otero Felipe for providing the ERA-Interim data.

## References

- R. Atkinson. Atmospheric chemistry of VOCs and  $\text{NO}_x$ . *Atmospheric Environment*, 34(12-14): 2063–2101, 2000.
- A. Baklanov, K. Schlünzen, P. Suppan, J. Baldasano, D. Brunner, S. Aksoyoglu, G. Carmichael, J. Douros, J. Flemming, R. Forkel, S. Galmarini, M. Gauss, G. Grell, M. Hirtl, S. Joffre, O. Jorba, E. Kaas, M. Kaasik, G. Kallos, X. Kong, U. Korsholm, A. Kurganskiy, J. Kushta, U. Lohmann, A. Mahura, A. Manders-Groot, A. Maurizi, N. Moussiopoulos, S. T. Rao, N. Savage, C. Seigneur, R. S. Sokhi, E. Solazzo, S. Solomos, B. Sørensen, G. Tsegas, E. Vignati, B. Vogel, and Y. Zhang.



355 Online coupled regional meteorology chemistry models in Europe: current status and prospects.  
 356 *Atmospheric Chemistry and Physics*, 14(1):317–398, 2014.

357 T. Butler, M. Lawrence, D. Taraborrelli, and J. Lelieveld. Multi-day ozone production potential  
 358 of volatile organic compounds calculated with a tagging approach. *Atmospheric Environment*, 45  
 359 (24):4082 – 4090, 2011.

360 W. P. L. Carter. Development of a Database for Chemical Mechanism Assignments for Volatile  
 361 Organic Emissions. *Journal of the Air & Waste Management Association*, 0, 2015.

362 W. P. L. Carter, A. M. Winer, K. R. Darnall, and J. N. P. Jr. Smog chamber studies of temperature  
 363 effects in photochemical smog. *Environmental Science & Technology*, 13(9):1094–1100, 1979.

364 J. Coates and T. M. Butler. A comparison of chemical mechanisms using tagged ozone production  
 365 potential (TOPP) analysis. *Atmospheric Chemistry and Physics*, 15(15):8795–8808, 2015.

366 J. P. Dawson, P. J. Adams, and S. N. Pandis. Sensitivity of ozone to summertime climate in the  
 367 eastern USA: A modeling case study . *Atmospheric Environment*, 41(7):1494 – 1511, 2007.

368 K. M. Emmerson and M. J. Evans. Comparison of tropospheric gas-phase chemistry schemes for  
 369 use within global models. *Atmospheric Chemistry and Physics*, 9(5):1831–1845, 2009.

370 L. K. Emmons, S. Walters, P. G. Hess, J.-F. Lamarque, G. G. Pfister, D. Fillmore, C. Granier,  
 371 A. Guenther, D. Kinnison, T. Laepple, J. Orlando, X. Tie, G. Tyndall, C. Wiedinmyer, S. L.  
 372 Baughcum, and S. Kloster. Description and evaluation of the Model for Ozone and Related  
 373 chemical Tracers, version 4 (MOZART-4). *Geoscientific Model Development*, 3(1):43–67, 2010.

374 W. S. Goliff, W. R. Stockwell, and C. V. Lawson. The regional atmospheric chemistry mechanism,  
 375 version 2. *Atmospheric Environment*, 68:174 – 185, 2013.

376 A. Guenther, T. Karl, P. Harley, C. Wiedinmyer, P. I. Palmer, and C. Geron. Estimates of global  
 377 terrestrial isoprene emissions using MEGAN (Model of Emissions of Gases and Aerosols from  
 378 Nature). *Atmospheric Chemistry and Physics*, 6(11):3181–3210, 2006.

379 A. B. Guenther, X. Jiang, C. L. Heald, T. Sakulyanontvittaya, T. Duhl, L. K. Emmons, and  
 380 X. Wang. The Model of Emissions of Gases and Aerosols from Nature version 2.1 (MEGAN2.1):  
 381 an extended and updated framework for modeling biogenic emissions. *Geoscientific Model  
 382 Development*, 5(6):1471–1492, 2012.

383 S. Hatakeyama, H. Akimoto, and N. Washida. Effect of temperature on the formation of  
384 photochemical ozone in a propene-nitrogen oxide (NO<sub>x</sub>)-air-irradiation system. *Environmental*  
385 *Science & Technology*, 25(11):1884–1890, 1991.

386 D. J. Jacob and D. A. Winner. Effect of climate change on air quality. *Atmospheric Environment*,  
387 43(1):51 – 63, 2009. Atmospheric Environment - Fifty Years of Endeavour.

388 D. J. Jacob, J. A. Logan, G. M. Gardner, R. M. Yevich, C. M. Spivakovsky, S. C. Wofsy,  
389 S. Sillman, and M. J. Prather. Factors regulating ozone over the United States and its export to  
390 the global atmosphere. *Journal of Geophysical Research*, 98(D8), 1993.

391 M. Jenkin, L. Watson, S. Utembe, and D. Shallcross. A Common Representative Intermediates  
392 (CRI) mechanism for VOC degradation. Part 1: Gas phase mechanism development. *Atmospheric*  
393 *Environment*, 42(31):7185 – 7195, 2008.

394 M. E. Jenkin, S. M. Saunders, and M. J. Pilling. The tropospheric degradation of volatile organic  
395 compounds: a protocol for mechanism development. *Atmospheric Environment*, 31(1):81 – 104,  
396 1997.

397 M. E. Jenkin, S. M. Saunders, V. Wagner, and M. J. Pilling. Protocol for the development of the  
398 Master Chemical Mechanism, MCM v3 (Part B): tropospheric degradation of aromatic volatile  
399 organic compounds. *Atmospheric Chemistry and Physics*, 3(1):181–193, 2003.

400 T. R. Karl and K. E. Trenberth. Modern global climate change. *Science*, 302(5651):1719–1723,  
401 2003.

402 J. J. P. Kuenen, A. J. H. Visschedijk, M. Jozwicka, and H. A. C. Denier van der Gon.  
403 TNO-MACC\_II emission inventory; a multi-year (2003–2009) consistent high-resolution european  
404 emission inventory for air quality modelling. *Atmospheric Chemistry and Physics*, 14(20):  
405 10963–10976, 2014.

406 K. A. Mar, N. Ojha, A. Pozzer, and T. M. Butler. WRF-Chem Simulations over Europe: Model  
407 Evaluation and Chemical Mechanism Comparison. *In Preparation*, 2016.

408 R. Mészáros, I. G. Zsély, D. Szinyei, C. Vincze, and I. Lagzi. Sensitivity analysis of an ozone  
409 deposition model. *Atmospheric Environment*, 43(3):663 – 672, 2009.

410 N. Otero, J. Sillmann, J. L. Schnell, H. W. Rust, and T. Butler. Synoptic and meteorological  
 411 drivers of extreme ozone concentrations over europe. *Environmental Research Letters*, 11(2):  
 412 024005, 2016.

413 N. Passant. Speciation of UK emissions of non-methane volatile organic compounds. Technical  
 414 report, DEFRA, Oxon, UK., 2002.

415 G. Pouliot, H. A. D. van der Gon, J. Kuenen, J. Zhang, M. D. Moran, and P. A. Makar. Analysis  
 416 of the emission inventories and model-ready emission datasets of Europe and North America for  
 417 phase 2 of the AQMEII project. *Atmospheric Environment*, 115:345–360, 2015.

418 S. E. Pusede, D. R. Gentner, P. J. Wooldridge, E. C. Browne, A. W. Rollins, K.-E. Min, A. R.  
 419 Russell, J. Thomas, L. Zhang, W. H. Brune, S. B. Henry, J. P. DiGangi, F. N. Keutsch, S. A.  
 420 Harrold, J. A. Thornton, M. R. Beaver, J. M. St. Clair, P. O. Wennberg, J. Sanders, X. Ren,  
 421 T. C. VandenBoer, M. Z. Markovic, A. Guha, R. Weber, A. H. Goldstein, and R. C. Cohen.  
 422 On the temperature dependence of organic reactivity, nitrogen oxides, ozone production, and  
 423 the impact of emission controls in San Joaquin Valley, California. *Atmospheric Chemistry and*  
 424 *Physics*, 14(7):3373–3395, 2014.

425 S. E. Pusede, A. L. Steiner, and R. C. Cohen. Temperature and Recent Trends in the Chemistry  
 426 of Continental Surface Ozone. *Chemical Reviews*, 115(10):3898–3918, 2015.

427 D. J. Rasmussen, J. Hu, A. Mahmud, and M. J. Kleeman. The ozone–climate penalty: Past,  
 428 present, and future. *Environmental Science & Technology*, 47(24):14258–14266, 2013. PMID:  
 429 24187951.

430 A. Rickard, J. Young, M. J. Pilling, M. E. Jenkin, S. Pascoe, and S. M. Saunders. The Master  
 431 Chemical Mechanism Version MCM v3.2. <http://mcm.leeds.ac.uk/MCMv3.2/>, 2015. [Online;  
 432 accessed 25-March-2015].

433 J. I. Rubin, A. J. Kean, R. A. Harley, D. B. Millet, and A. H. Goldstein. Temperature dependence  
 434 of volatile organic compound evaporative emissions from motor vehicles. *Journal of Geophysical*  
 435 *Research: Atmospheres*, 111(D3), 2006. D03305.

436 R. Sander, A. Kerkweg, P. Jöckel, and J. Lelieveld. Technical note: The new comprehensive  
 437 atmospheric chemistry module mecca. *Atmospheric Chemistry and Physics*, 5(2):445–450, 2005.

438 S. M. Saunders, M. E. Jenkin, R. G. Derwent, and M. J. Pilling. Protocol for the development of  
 439 the Master Chemical Mechanism, MCM v3 (Part A): tropospheric degradation of non-aromatic  
 440 volatile organic compounds. *Atmospheric Chemistry and Physics*, 3(1):161–180, 2003.

441 J. L. Schnell, M. J. Prather, B. Josse, V. Naik, L. W. Horowitz, P. Cameron-Smith, D. Bergmann,  
 442 G. Zeng, D. A. Plummer, K. Sudo, T. Nagashima, D. T. Shindell, G. Faluvegi, and S. A. Strode.  
 443 Use of north american and european air quality networks to evaluate global chemistry–climate  
 444 modeling of surface ozone. *Atmospheric Chemistry and Physics*, 15(18):10581–10596, 2015.

445 S. Sillman. The use of NO<sub>y</sub>, H<sub>2</sub>O<sub>2</sub>, and HNO<sub>3</sub> as indicators for ozone-NO<sub>x</sub>-hydrocarbon sensitivity  
 446 in urban locations. *Journal of Geophysical Research: Atmospheres*, 100(D7):14175–14188, 1995.

447 S. Sillman. The relation between ozone, NO<sub>x</sub> and hydrocarbons in urban and polluted rural  
 448 environments. *Atmospheric Environment*, 33(12):1821 – 1845, 1999.

449 S. Sillman and P. J. Samson. Impact of temperature on oxidant photochemistry in urban,  
 450 polluted rural and remote environments. *Journal of Geophysical Research: Atmospheres*, 100  
 451 (D6):11497–11508, 1995.

452 D. Simpson, A. Benedictow, H. Berge, R. Bergström, L. D. Emberson, H. Fagerli, C. R. Flechard,  
 453 G. D. Hayman, M. Gauss, J. E. Jonson, M. E. Jenkin, A. Nyíri, C. Richter, V. S. Semeena,  
 454 S. Tsyro, J.-P. Tuovinen, Á. Valdebenito, and P. Wind. The EMEP MSC-W chemical transport  
 455 model – technical description. *Atmospheric Chemistry and Physics*, 12(16):7825–7865, 2012.

456 A. L. Steiner, S. Tonse, R. C. Cohen, A. H. Goldstein, and R. A. Harley. Influence of future  
 457 climate and emissions on regional air quality in California. *Journal of Geophysical Research:*  
 458 *Atmospheres*, 111(D18), 2006. D18303.

459 W. R. Stockwell, P. Middleton, J. S. Chang, and X. Tang. The second generation regional acid  
 460 deposition model chemical mechanism for regional air quality modeling. *Journal of Geophysical*  
 461 *Research: Atmospheres*, 95(D10):16343–16367, 1990.

462 W. R. Stockwell, F. Kirchner, M. Kuhn, and S. Seefeld. A new mechanism for regional atmospheric  
 463 chemistry modeling. *Journal of Geophysical Research: Atmospheres*, 102(D22):25847–25879,  
 464 1997.

465 E. von Schneidemesser, P. S. Monks, J. D. Allan, L. Bruhwiler, P. Forster, D. Fowler, A. Lauer,

466 W. T. Morgan, P. Paasonen, M. Righi, K. Sindelarova, and M. A. Sutton. Chemistry and the  
467 Linkages between Air Quality and Climate Change. *Chemical Reviews*, 2015. PMID: 25926133.

468 E. von Schneidemesser, J. Coates, A. J. H. Visschedijk, H. A. C. Denier van der Gon, and T. M.  
469 Butler. Variation of the NMVOC speciation in the solvent sector and the sensitivity of modelled  
470 tropospheric ozone. *Atmospheric Environment*, Submitted for Publication, 2016.

471 P. Wagner and W. Kuttler. Biogenic and anthropogenic isoprene in the near-surface urban  
472 atmosphere — A case study in Essen, Germany. *Science of The Total Environment*, 475:104 –  
473 115, 2014.

474 G. Yarwood, S. Rao, M. Yocke, and G. Z. Whitten. Updates to the Carbon Bond Chemical  
475 Mechanism: CB05. Technical report, U. S Environmental Protection Agency, 2005.